Resonant Acoustic Sensor System for the Wireless Monitoring of Injection Moulding

F. Müller[1], P. O'Leary[2], G. Rath[2], C. Kukla[3], M. Harker[2], T. Lucyshyn[1] and C. Holzer[1]

[1]*Chair of Polymer Processing, Montanuniversitaet Leoben, Otto Gloeckel-Strasse 2, Leoben, Austria*
[2]*Chair of Automation, Montanuniversitaet Leoben, Leoben, Austria*
[3]*Industrial Liasion Department, Montanuniversitaet Leoben, Leoben, Austria*
{*florian.mueller, paul.oleary, gerhard.rath, christian.kukla, matthew.harker,
thomas.lucyshyn, clemens.holzer*}*@unileoben.ac.at*

Abstract: The production of high quality plastic parts requires in-mould sensors to monitor the injection moulding process. A novel wireless sensor concept is presented where structure borne sound is used to transmit information from the inside of an injection mould to the outside surface, eliminating the need for cabling within the mould. The sound is acquired and analyzed using new algebraic basis function techniques to enable the detection of temporal occurrence of frequency patterns in the presence of large levels of noise. The temporal occurrence of the resonators represents the passing melt front. The reduction of spectral leakage is computed by an alternative method using low degree Gram polynomials. The computation of the pattern matching algorithm yields both the correlation coefficients and their covariances which are used to determine the certainty of the measurement. The paper presents the used mathematical background as well as real measurements performed on an injection moulding machine. A test mould was equipped with two different resonant structures. Besides calculating the correlation coefficients the 3σ confidence interval of the coefficients is computed. With the novel algebraic approach a reliable separation of the two temporal points of occurrence of the resonant structures was computed.

1 INTRODUCTION

Injection moulding is the most important manufacturing process for plastic parts. In this highly dynamic process a lot of effort went into the development of the control algorithms of the injection moulding machine concerning repeatability (Chen and Turng, 2005; Giboz et al., 2007; Kamal et al., 1984). In contrast the injection mould is often neglected in terms of implementing control elements in form of sensors. There are mainly two types of in-mould sensors that are common, cavity wall temperature- and pressure-sensors (Giboz et al., 2007) which always transmit the measured values by wires. Since wires have some disadvantages concerning mould design and maintenance effort (Zhang et al., 2005), current research in the field of wireless in-mould sensors presents different approaches (Bulst et al., 2001; Gao et al., 2008; Zhang et al., 2005).

In this paper a different approach is shown where no active circuitry within the mould is required (Müller et al., 2012). A distinctive structure borne sound is generated on purpose by a mechanical resonator which is excited by the passing melt front. Hence, the temporal event when the melt front passes the resonator can be detected. This temporal resolution of the passing melt front is of special interest for example for detecting the switch over point (from filling to holding pressure phase) or for hot runner balancing (Kazmer et al., 2010; Frey, 2004).

The main contributions of this paper are:

1. A new sensor concept is presented for wireless monitoring of the filling of moulds during injection moulding;

2. Structure borne sound is used to implement wireless transmission of information from multiple positions to a single accelerometer mounted outside the mould. This eliminates the need for cabling within the mould, making the mould both cheaper in construction and simpler to service;

3. The design of a mechanical resonator is combined with a new signal processing method to enable the detection of multiple events in the single time

varying signal;

4. A new algebraic approach to the implementation of frequency domain pattern matching is presented. The new approach yields a numerically very efficient solution to computing the desired correlation coefficients. Furthermore and very important for measurements in an industrial environment, the new method also yields a method for estimating the covariance of the correlation coefficients. Consequently, the detection of an event can be made with a given certainty.

2 PRINCIPLE OF OPERATION

The aim is to develop a system which is capable of detecting when the melt front reaches specific regions in a mould, i.e. the detection of discrete temporal events. Multiple detections should be possible and there is the further desire not to have any cabling within the mould. This makes the mould simpler in construction and easier to service. The principle of operation is very simple, see Figure 1: The dark portion in the figure represents the melt (A) filling the cavity (B). When the melt reaches the pin (C) it is depressed and excites the resonator (D), which injects a characteristic sound into the metal mass of the mould. This portion of the system is purely mechanical. The sound is acquired using a single accelerometer and analyzed.
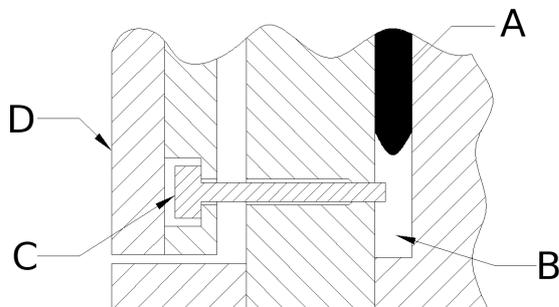

Figure 1: Schematic drawing of the principle of operation. The dark portion (A) represents the melt filling the cavity (B). When the melt reaches the pin (C) it is depressed and excited the resonator (D). This portion of the system is purely mechanical (Müller et al., 2012).

The sensor system consists of three main portions:

1. Mechanical resonators, these are purely mechanical devices which exhibit a characteristic damped oscillatory behaviour. When excited they resonate and introduce structure borne sound into the metallic mass of the mould.

2. A single accelerometer mounted on the outside of the mould. This accelerometer detects the struc-

tural borne sound from all the mechanical resonators.

3. A signal acquisition and processing unit, which acquires the signal from the accelerometer and implements a new matrix algebraic approach to pattern recognition. The system enables the detection of the time points of excitation of the different mechanical resonators and with this the detection of the melt front at the desired points in the mould.

This paper presents the development of the complete detection system.

2.1 Mechanical Resonator

In Figure 2 a rendered section view of a mechanical resonator is shown. The system consists of: a sprung movable pin (A and B), and a resonant body (C). The spring ensures the pin is in the correct position prior to excitation. When the melt reaches the position in the mould where the pin is, it accelerates the pin and excites the resonant body. The pin, spring and resonant body form a damped resonator which emits a characteristic acoustic signal into the metallic body of the mould.
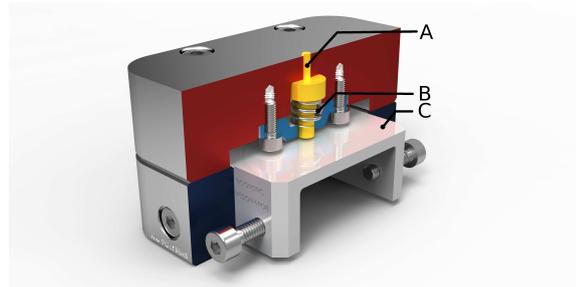

Figure 2: Rendered section view of one of the implemented mechanical resonators. The pin (A) which is pushed by the melt, the spring (B) which positions the pin and the resonant body (C). This Figure shows the implemented 12 [kHz] resonator (Müller et al., 2012).

Two different resonator designs were implemented for test purposes[1]:

1. A plate resonator, as shown in Figure 2, with a primary resonant mode at 12 [kHz], and

2. a tongue resonator, not shown, with a primary resonant mode at 3.8 [kHz].

Both designs use the same mechanical components (housing, pin and spring), only the resonant body is exchanged. In this manner different resonant characteristics can be simply implemented. The different

---

[1]For simplicity in the rest of the paper the two resonators are identified by their primary modal frequency.

oscillatory characteristics enable the separation of the events from the different resonators in the signal acquired from one and the same accelerometer.

2.2 Acoustic Detection

A single accelerometer is mounted on the outside of the mould. It detects the structure borne sounds from all the resonators. The accelerometer (352A60 from PCB Piezotronics) has a frequency range from $5-60000\,[\mathrm{Hz}]$ and was sampled[2] with $f_s = 120\,[\mathrm{kHz}]$. The high frequency range has been chosen to improve the performance of the system in the presence of significant acoustic disturbances associated with the operation of the machine.

The high sampling frequency gives a larger number of spectral components which can be used in the pattern recognition to detect the desired oscillations. The resonators have multiple harmonics which yield multiple correlated components in the frequency domain. However, the wider range of noise acquired with the higher sampling frequency is uncorrelated. Consequently, a better signal to noise ratio can be achieved in this manner. The signal acquisition is synchronized with the start of the injection process.

2.3 Signal Processing

The aim of the signal processing is to implement optimal detectors, optimal in terms of noise performance, for the characteristic oscillations of the resonators. Due to the complex mechanical form and internal reflections within the mould, the signals from the resonators are not fully orthogonal. Consequently classical correlation detectors (Fano, 1951) will not function optimally. This paper presents a new algebraic approach to signature recognition, which is numerically efficient, while maintaining the advantages of full spectrum pattern matching. In addition to the matching of the pattern the new method also implements the covariance propagation, which in turn yields a confidence interval. Consequently, the certainty of the measurement is also determined. The details are presented in the following section.

3 MATHEMATICAL FRAMEWORK

In this paper a new algebraic implementation of a frequency domain signature matching is implemented.

There are two steps involved in signature matching:

1. Signature identification, i.e. identifying the optimal frequency domain signatures for each resonator. This task is performed a-priori to the measurement and can be considered as a calibration of the system.

2. Signature matching, which is formulated as a linear matrix algebraic computation. This method is numerically efficient and the covariance propagation for the linear operator can be computed.

Before proceeding to these two steps it is necessary to introduce a matrix algebraic approach to computing a discrete Fourier transform (DFT) and a new method for reducing the effects of the Gibbs phenomena. In most common literature on digital signal processing, e.g., (Press et al., 2002; Oppenheim and Schafer, 1989), the computation of the DFT is formulated as,

$$s(k) = \sum_{n=0}^{N-1} y(n)\,\mathrm{e}^{-j2\pi kn/N} \qquad (1)$$

whereby, $y(n)$ is the nth sample of the input signal, N is the total number of samples available, and k defines the discrete frequency $f_k = (2\pi kn/N)\,f_s$, with respect to the sampling frequency f_s. Given N input samples there are N components in the discrete Fourier spectrum. Computing the discrete Fourier series is most commonly called the discrete Fourier transform and is most commonly implemented using the fast Fourier transform (FFT) algorithm. The FFT and DFT are functionally identical, the FFT is simply a numerically more efficient method of performing the computation.

The computation of the DFT can also be formulated as a matrix[3] operation. The discrete Fourier basis functions $f(k)$,

$$f(k) \triangleq \mathrm{e}^{-j2\pi kn/N}, \qquad (2)$$

can be concatenated forming the columns of a matrix F, such that[4],

$$\mathsf{F} \triangleq \left[f(0), \dots, f(N-1) \right]. \qquad (3)$$

Now given a vector y of N input samples, the complete spectrum s, a vector, of the signal y is computed as,

$$\mathsf{s} = \mathsf{F}\,\mathsf{y}. \qquad (4)$$

Computing the discrete Fourier spectrum in this manner is significantly less efficient than computing an

---

[2]For test purposes the signal was acquired using a data acquisition box from National Instruments (USB-6366).

[3]A brief note on nomenclature: matrices are indicated by *sanserif* capital letters, e.g. H, and vectors by sanserif lowercase letters, e.g. y.

[4]The matrix F can be generated in MATLAB using the code, $\mathsf{F} = \mathrm{dftmtx}(N)'$.

FFT if finally all spectral components are required. However, as shall be seen, given the need to only identify a low number of signatures the method offers significant advantages, both with respect to numerical efficiency as also in estimating confidence intervals.

Prior to computing the spectrum it is necessary to take measures so as to limit the errors associated with the Gibbs phenomena. The classical approach is to use windowing (Press et al., 2002; Lindquist, 1988), however, a new method based on polynomial approximation was introduced recently, see (O'Leary and Harker, 2011) for derivations and exact nature of the computation. The signal is projected onto the orthogonal complement of a set of Gram polynomial basis functions of low degree. The Gram polynomial basis functions up to degree d are also used to form the columns of a matrix G_d, the projection P onto the orthogonal complement can be computed as,

$$P = I - G_d G_d^T, \qquad (5)$$

where I is the unit matrix.

The spectrum with reduced spectral leakage is now computed as,

$$s = F \left\{ I - G_d G_d^T \right\} y. \qquad (6)$$

It should be noted that, $H \triangleq F \left\{ I - G_d G_d^T \right\}$ is once again a matrix. In this manner reducing the Gibbs effect has added no additional numerical complexity, since H can be computed a-priori.

3.1 Signature Identification

The calibration procedure takes advantage of superposition, in the assumption that the noise of the machine and the sound from the resonator can be regarded as additive signals. The ith resonator alone is artificially activated while the machine is not running. The signal from the accelerometer is acquired and the corresponding spectrum is computed,

$$s_i = H y. \qquad (7)$$

This procedure is repeated for each resonator yielding a set of n initial spectral signatures one for each resonator. Unfortunately, due to the complicated mechanical forms and internal acoustic reflections within the form these vectors are not fully orthogonal.

The orthogonality of the signatures is achieved by projecting them onto their mutual orthogonal complements. Given n signatures this is computed as,

$$\hat{s}_i = \left\{ I - \left(\sum_k s_k s_k^T \right) \right\} s_i \ \ \forall \ k \in [1 \dots n], k \neq i. \qquad (8)$$

To support understanding it is helpful to formulate this computation for two signatures,

$$\hat{s}_1 = s_1 - s_2 s_2^T s_1 = \left(I - s_2 s_2^T \right) s_1 \qquad (9)$$

$$\hat{s}_2 = s_2 - s_1 s_1^T s_2 = \left(I - s_1 s_1^T \right) s_2. \qquad (10)$$

This computation yields a set of n orthogonalized signatures $\hat{s}_i$, which are complex vectors each of length N. These are then used in the signature matching process. The matrix of signatures S is formed by concatenating the individual orthogonalized vectors and dividing them by their norm,

$$S = \left[\frac{\hat{s}_1}{|\hat{s}_1|}, \dots, \frac{\hat{s}_n}{|\hat{s}_n|} \right]. \qquad (11)$$

In this manner the matrix S has a unitary norm. Consequently, S^+, which is discussed next, has also a unitary norm.

The orthogonalization process described by Equations 9 and 10 have worked well with the sensors used in the experiment presented in this paper. However, other experiments suggest that a diagonalisation of the matrix of signatures, using singular value decomposition, yields an even better separation of the signals with a lower cross sensitivity. This issue, however, is still the subject of further investigation.

3.2 Signature Matching

To support understanding it is helpful to take a more fundamental look at the nature of the system and the computation being performed. The excitation of the pin can be approximated as a dirac pulse, in this case the signatures correspond to the impulse response of the resonators. For simplicity the orthogonalization process is not considered now. The impulse response corresponds to the first eigenfunction of the differential equation describing the dynamics of the resonator. Given a measurement of the resonator's response, with the addition of noise, the task is to perform de-convolution of the measured signal with the response of the differential equation. This is fundamentally an inverse problem. In a lose sense it is equivalent to inversion of the stochastic differential equation for the system.

An algebraic approach to the computation has been chosen since the Moore-Penrose pseudo-inverse (Golub and Van Loan, 1996) provides a least square approximation for the inversion of a rectangular matrix,

$$S^+ \triangleq \left(S^T S \right)^{-1} S^T, \qquad (12)$$

which ensures,

$$S^+ S = I. \qquad (13)$$

Computing S^+ is akin to inverting the eigenfunctions s_i contained in S which describe the differential equations of the resonators.

The input signal is continually acquired and a subset of N values are selected to form the vector y. The spectrum of the signal is computed as shown in Equation 6,

$$\mathsf{s}_t = \mathsf{H}\,\mathsf{y}. \tag{14}$$

This is called the temporal varying signature s_t. It should be noted that it may contain zero or any number of the sought events. The correlation coefficient to the n signatures is computed as,

$$\mathsf{c} = \mathsf{S}^+\mathsf{s}_t = \mathsf{S}^+\mathsf{H}\,\mathsf{y}, \tag{15}$$

where c is an n element column vector[5,6]. The matrix L can now be defined as $\mathsf{L} \triangleq \mathsf{S}^+\mathsf{H}$, this is of size $N \times n$, in the test case here $n = 2$ and $N = 600$. This matrix is computed a-priori to measurement; consequently computing the correlation coefficients at runtime is numerically very efficient and can be written as,

$$\mathsf{c} = \mathsf{L}\,\mathsf{y}. \tag{16}$$

The computation is repeated p samples later. Computation in this manner is very closely related to the short-time Fourier transform (STFT). For those more familiar with classical digital signal processing: the columns of L can be considered to be the coefficients of a finite impulse response (FIR) filter (Oppenheim and Schafer, 1989), with a decimation factor p. Consequently, there is a bank of n FIR filters given n resonators.

3.3 Covariance Propagation

The covariance (Brandt, 1998) for a vector is defined as,

$$\Lambda_c \triangleq \{\mathsf{c} - \mathrm{E}(\mathsf{c})\}\{\mathsf{c} - \mathrm{E}(\mathsf{c})\}^T. \tag{17}$$

Now substituting the relationship $\mathsf{c} = \mathsf{L}\,\mathsf{y}$, yields,

$$\Lambda_c = \{\mathsf{L}\,\mathsf{y} - \mathsf{L}\,\mathrm{E}(\mathsf{y})\}\{\mathsf{L}\,\mathsf{y} - \mathsf{L}\,\mathrm{E}(\mathsf{y})\}^T, \tag{18}$$

and factoring out L,

$$\Lambda_c = \mathsf{L}\{\mathsf{y} - \mathrm{E}(\mathsf{y})\}\{\mathsf{y} - \mathrm{E}(\mathsf{y})\}^T\,\mathsf{L}^T. \tag{19}$$

---

[5]To facilitate numerical efficiency the correlation coefficients can be computed as,

$$\mathsf{c} = \mathsf{S}^+ abs(\mathsf{H}\mathsf{y}).$$

The norm of $\left|\mathsf{S}^+\right|$ is 1 and the norm of $|\mathsf{H}| = 1 - 2/n$, in the application $n = 600$, therefor $|\mathsf{H}| \approx 1$. Consequently, this numerical simplification does not change the norm of the result.

[6]Ideally this computation should yield only real values for c; however, due to numerical errors small imaginary components may remain. For this reason, it is suggested to take only the real portion, i.e., $\mathcal{R}(\mathsf{c})$.

By definition $\Lambda_y \triangleq \{\mathsf{y} - \mathrm{E}(\mathsf{y})\}\{\mathsf{y} - \mathrm{E}(\mathsf{y})\}^T$, consequently,

$$\Lambda_c = \mathsf{L}\,\Lambda_y\,\mathsf{L}^T. \tag{20}$$

If we can regard the input noise to the system as independent identically distributed (i.i.d.) Gaussian errors with standard deviation σ, the covariance of the input is given by,

$$\Lambda_y = \sigma^2\,\mathsf{I}, \tag{21}$$

and consequently,

$$\Lambda_c = \sigma^2\,\mathsf{L}\,\mathsf{L}^T. \tag{22}$$

In this manner we also have an estimator for the covariance of the correlation coefficients. This is one of the major advantages of using an algebraic approach to solve this problem. No other computation method would yield the covariance estimates in such a simple manner.

3.4 Decision Process

Given the vector of correlation coefficients c and the associated covariance matrix Λ_c: a decision with a desired confidence interval can be made.

There is a delay of N samples for the first decision and then a decision follows every P samples. The group delay for an FIR filter with N symmetric coefficients is $t_d = N/(2f_s)$, for example in this application with $f_s = 120\,[\mathrm{kHz}]$ and a signature length of $N = 600$ there is a decision delay of $t_d = 2.5\,[\mathrm{ms}]$ and a new decision is available every $t_r = 0.42\,[\mathrm{ms}]$.

4 EXPERIMENTAL SETUP AND RESULTS

The experiments were performed on an Arburg injection moulding machine (470A-1000) with a Poly-Propylen (C7069-100NA) from Dow. The injection speed was set to $60\,[\mathrm{cm}^3\mathrm{s}^{-1}]$. The diameter of the injection screw is $40\,[\mathrm{mm}]$. For the measurements a test mould was built. The mould consists of two symmetrical cavities which are gated by a hot runner system (Johannaber and Michaeli, 2004). The hot runner system is equipped with an electromagnetic valve gate control. Two test resonators with different designs were implemented and installed in the test mould.

Figure 3 shows a picture of the clamped mould in the injection moulding machine. The mould is shown in the opened position. During processing the mould is closed and charged with a clamping force of approximately $900\,[\mathrm{kN}]$. The two symmetric cavities are indicated by A and B. The accelerometer in the picture is marked with C, which is mounted on the outside surface of the mould.
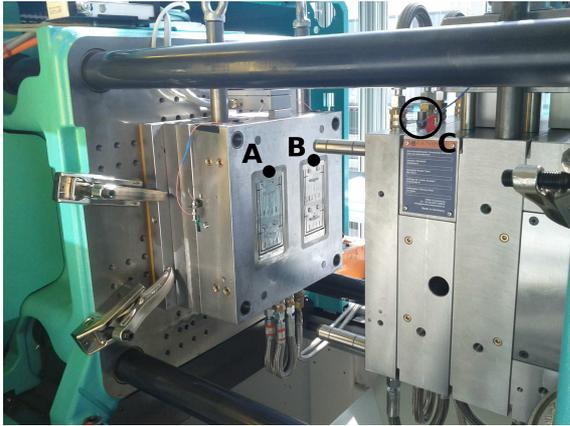
Figure 3: Picture of the mould clamped in the injection moulding machine. The mould is shown in opened position. During the production process the mould is closed and charged with a clamping force of approximately 900 [kN]. A and B indicate the two symmetrical cavities; C marks the position of the accelerometer mounted on the outside surface of the mould.

4.1 Experimental Signature Identification

The machine is not running during identification of the signatures. This reduces the spurious presence of noise during this process. Since there are two resonators implemented in the mould $n = 2$. As previously mentioned a sampling frequency of $f_s = 120 [kHz]$ was used. Both resonators were excited independently and their time response was measured. In Figure 4 the time response as a function of time for both resonators is shown. It is important to note that the resonator nominally designed for $3.8 [kHz]$ has many overtones which lead to higher frequency components than the $12 [kHz]$ resonator.

The sampled data was segmented into packets containing $N = 600$ samples. Each packet is projected onto the orthogonal complement of a Gram polynomial G_d of degree $d = 1$ prior to computing the corresponding discrete Fourier spectrum, this suppresses significant portions of the spectral leakage. The obtained signatures are not fully orthogonal due to the complex mechanical form of the mould as well as acoustic reflections inside it.

Therefore the two signatures are then orthogonalized according to Equations 9 and 10. The resulting orthogonalized signatures are shown in Figure 5. Since the magnitude spectrum of a real signal is symmetric, only the first $N/2$, i.e., 300 values are shown.

From the spectrum it gets clear, that there are just significant frequency components up to approximatly $20 [kHz]$. With a given sampling rate of $120 [kHz]$
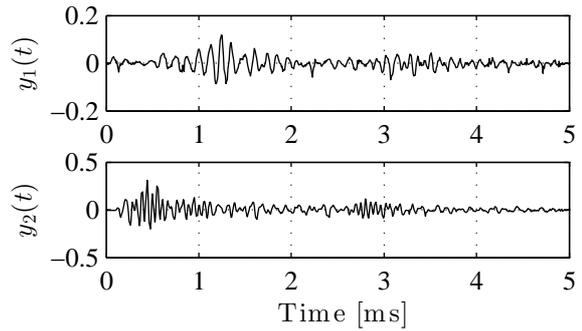

Figure 4: Top: the time response of the $12 [kHz]$ resonator. Bottom: the time response of the $3.8 [kHz]$ resonator. It is important to note that the resonator nominally designed for $3.8 [kHz]$ has many overtones. This lead to higher frequency components. Each of the time signatures consists of 600 samples. The shown results were measured independently and are not shown synchronized.

this means that just the first 50 values of the spectrum are required for event identification. Since the noise is distributed over 600 values of the spectrum and just 50 of them are needed, this corresponds to an implicit regularization. This yields a noise gain of $g_n = \sqrt{50/600}$.

The two orthogonalized signatures, $\hat{s}_1(\omega)$ and $\hat{s}_2(\omega)$, are used during further processing.
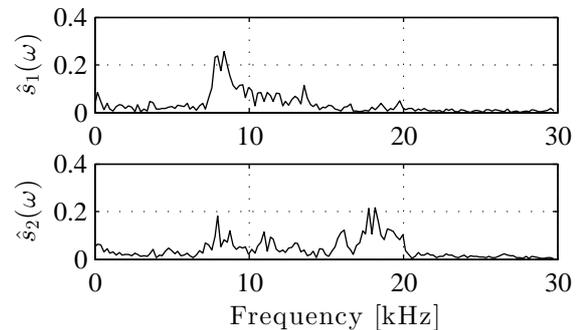

Figure 5: Top: the spectrum of the impulse response of the $12 [kHz]$ resonator. Bottom: the spectrum of the impulse response of the $3.8 [kHz]$ resonator. Here, as in Figure 4, the higher frequency components associated with the harmonics of the $3.8 [kHz]$ are visible in the spectrum. Note there are only significant magnitudes in the range up to approximately $20 [kHz]$. Given the sampling frequency of $120 [kHz]$ this means only 50 components are required to identify the events. This corresponds to an implicit regularization, the noise is distributed over 600 of which only 50 are used. This yields a noise gain of $g_n = \sqrt{50/600}$.

4.2 Experimental Signature Matching

During signature matching the machine is running and the process is subject to large levels of spurious noise emitted from the mechanisms of the injection

moulding machine and process. At the beginning of the injection moulding cycle the valves are opened which results in a large excitation of the time signal at the beginning of the measurement (see beginning of Figure 6). Despite having a fully symmetrical flow channel system there will be an unbalanced filling of the cavities, having tolerances and inhomogeneous temperature distributions (Johannaber and Michaeli, 2004). To compensate the unbalanced filling and ensure simultaneous filling of both cavities the valves are opened consecutively whereby the opening delay is controlled by a closed loop controller. In each of the cavities a resonator is implemented, the left cavity with the 12 [kHz] resonator, the right one with the 3.8 [kHz] resonator.

The measurements were synchronized to the start of the injection moulding process. The data acquisition box records the accelerometer channels for a duration of 10 [s]. The first 2 [s] of the recorded signal are shown in Figure 6. It can be seen that the signal is perturbed with large levels of noise. It is assumed that the noise is distributed as i.i.d. Gaussain noise with $\sigma = 1.6e-4$.
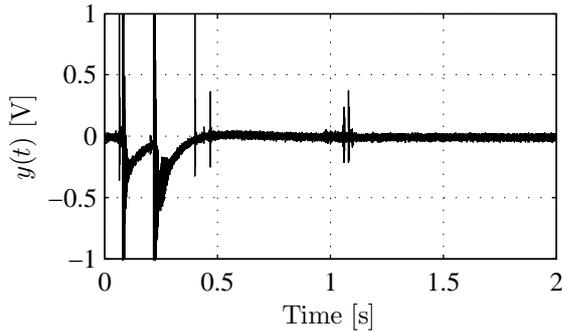

Figure 6: First 2 [s] of recorded accelerometer signal shown in time domain. The signal is perturbed with noise over the whole measurement. The noise is assumed as i.i.d Gaussian noise, $\sigma = 1.6e-4$. The searched resonators both appear in the time domain at approximately 1.1 [s] after start of the filling phase. The exact time point is estimated with the correlation coefficient computation.

To support understanding, the short time Fourier transform (Spectrogram) of the signal is computed and shown in Figure 7. Thereby just the period where the frequency patterns are expected is shown in the spectrogram. At approximately 1.06 [s] the 12 [kHz] resonator is found, at approximately 1.08 [s] the 3.8 [kHz] resonator. The temporal positions of the events were identified using signature matching, i.e. via the correlation coefficients which are discussed later. This visualization is not required during normal operation.

The correlation coefficients were computed as proposed in Equation 15 and are shown with a
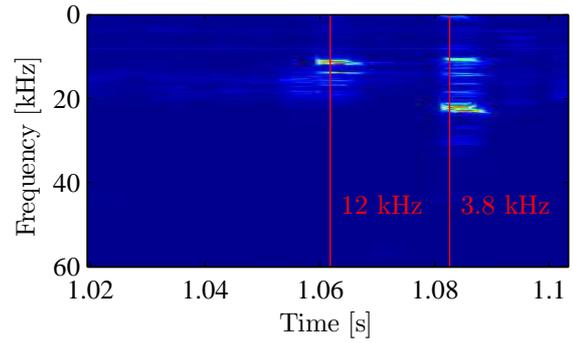

Figure 7: Magnitude spectrogram of the accelerometer signal, in addition the time points when the resonator events occurred are shown, for both the 3.8 [kHz] and 12 [kHz] resonators. The temporal positions of the events were identified using the signature matching, i.e. via the correlation coefficients.

3σ (99.73 %) confidence interval in Figure 8 (middle: $c_1(t)$ for the 12 [kHz] resonator; bottom: $c_2(t)$ for the 3.8 [kHz] resonator). The top diagram shows the recorded data $y(t)$ in the time domain.

Regarding $c_1(t)$, the solid black line indicates the computed coefficients. In addition, a gray band indicates the 3σ (99.73 %) confidence interval. The confidence interval is calculated by the covariance matrix Λ_c, which is computed after Equation 22 as,

$$\Lambda_c = \begin{bmatrix} 0.91630 & 0.79795 \\ 0.79795 & 0.91630 \end{bmatrix}. \tag{23}$$

Since the matrix Λ_c is symmetric and has the identical values in the diagonal, a symmetric 3σ (99.73 %) confidence interval for both components, i.e. $c_1(t)$ and $c_2(t)$, is calculated as ± 2.8.

The value of c_1, corresponding to the 12 [kHz] resonator, stays at a low level up to 1.059 [s] where a peak appears. At 1.061 [s] a black vertical line indicates the detection of the 3.8 [kHz] resonant structure. The detection is computed with descriptive statistics [7] (Haase, 2002).

The second correlation coefficient c_2, corresponding to the 3.8 [kHz] resonator, shows a peak starting at 1.080 [s]. The temporal occurrence event was recognized at 1.082 [s].

For both detection events a cross correlation can be observed. Since the cross correlations are small compared to the peak values of c a reliable separation of both events can be ensured.

Figure 8 (top) shows the time domain signal $y(t)$ of the recorded accelerometer data with indicated events for both resonant structures. It has to be noted

---

[7] Mainly the calculation of the standard deviation and the skewness as well as a probability density function are used for computing the detection.
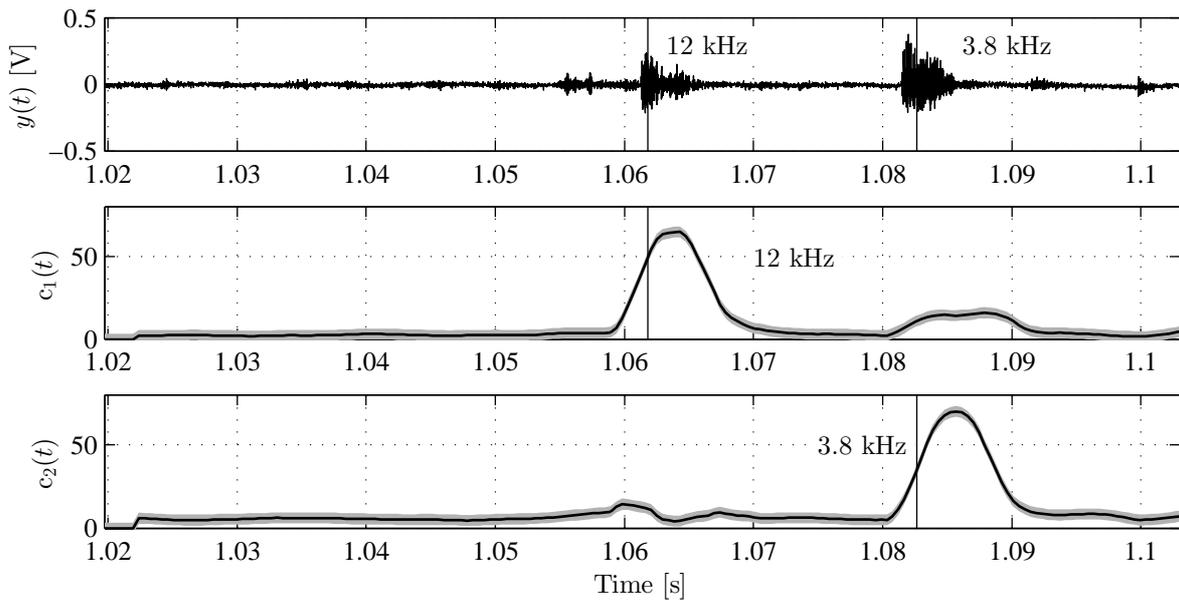
Figure 8: top: amplitude signal $y(t)$ from the accelerometer, the time points for the identification of the two events are also shown. Middle: the black line shows the correlation coefficient $c_1(t)$ for the $12\,[\text{kHz}]$ resonator as a function of time, the gray region around the line is the 3σ, i.e., 99.73%, confidence interval for the correlation. Bottom: the black line shows the correlation coefficient $c_2(t)$ for the $3.8\,[\text{kHz}]$ resonator as a function of time, the gray region around the line is the 3σ, i.e., 99.73%, confidence interval for the correlation. Some cross sensitivity of the correlations can be observed. However, they are sufficiently small to ensure a reliable separation of the two events.

that the coefficients c both start rising slightly before the deflection of the time domain signal. This lead from the fact that the signal is segmented into packets. These packets are evaluated at their center point.

In terms of the injection moulding process the temporal detection point of the resonant structures indicate the passing melt front.

5 CONCLUSIONS

In this paper a novel wireless in-mould sensor for injection moulding was presented. The sensor is capable to detect the melt front at certain predefined positions in the cavity. The data transmission is obtained by the generation of distinctive sound which is detected by an outside mould surface mounted accelerometer. To separate multiple implemented sensors a frequency pattern search is performed using a new linear algebraic approach. This method yields a numerically efficient approach for computing the correlation coefficients. In addition, the covariance propagation can be estimated which consequently yields the computation of a confidence interval of the estimated coefficients.

The proposed sensor system and the signal processing were tested on an injection moulding machine. In the mould, two different resonant structures

were implemented. First the process of signature identification was described. The obtained orthogonalized signatures were used for the pattern matching process. Injection moulding cycles were recorded with an outside mounted accelerometer. The recorded signal contains the sound of the resonators which is superposed with large levels of noise from the machine, the mould and auxiliary units. However, the described frequency domain pattern matching algorithm was able to find both temporal points when the resonant structures were excited. The detection of the resonant structures corresponds to the detection of the temporal moment of the passing melt front. In addition, the 3σ confidence interval of the computed correlation coefficients was shown.

The process of orthogonalization of the signatures yields space for further investigation with respect to perturbation analysis, i.e. achieving optimal sensitivity for noise.

REFERENCES

Brandt, S. (1998). *Data Analysis: Statistical and Computational Methods for Scientists and Engineers.* Springer, Berlin, 3rd edition.

Bulst, W.-E., Fischerauer, G., and Reindl, L. (2001). State of the art in wireless sensing with surface acoustic

waves. *IEEE Transactions on Industrial Electronics*, 48(2):265–271.

Chen, Z. and Turng, L.-S. (2005). A review of current developments in process and quality control for injection molding. *Advances in Polymer Technology*, 24(3):165–182.

Fano, R. (1951). *Signal-to-noise Ratio in Correlation Detectors*. Technical report (Massachusetts Institute of Technology. Research Laboratory of Electronics). Massachusetts Institute of Technology, Research Laboratory of Electronics.

Frey, J. (2004). Method for automatically balancing the volumetric filling of cavities. US Patent 2004/0113303 A1.

Gao, R., Fan, Z., and Kazmer, D. (2008). Injection molding process monitoring using a self-energized dual-parameter sensor. *CIRP Annals - Manufacturing Technology*, 57(1):389–393.

Giboz, J., Copponnex, T., and Mélé, P. (2007). Microinjection molding of thermoplastic polymers: a review. *Journal of Micromechanics and Microengineering*, 17(6):96–109.

Golub, G. and Van Loan, C. (1996). *Matrix Computations*. The Johns Hopkins University Press, Baltimore, 3rd edition.

Haase, S. (2002). *Spectral and statistical methods for vibration analysis in steel rolling*. PhD Thesis Montanuniversitaet Leoben.

Johannaber, F. and Michaeli, W. (2004). *Handbuch Spritzgiessen*. Hanser, München, 2nd edition.

Kamal, M. R., Patterson, W. I., Fara, D. A., and Haber, A. (1984). A study in injection molding dynamics. *Polymer Engineering and Science*, 24(9):686–691.

Kazmer, D. O., Velusamy, S., Westerdale, S., Johnston, S., and Gao, R. X. (2010). A comparison of seven filling to packing switchover methods for injection molding. *Polymer Engineering & Science*, 50(10):2031–2043.

Lindquist, C. S. (1988). *Adaptive and Digital Signal Processing with Digital Filtering Applications*. Steward & Sons.

Müller, F., Rath, G., Lucyshyn, T., Kukla, C., Burgsteiner, M., and Holzer, C. (2012). Presentation of a novel sensor based on acoustic emission in injection molding. *Journal of Applied Polymer Science*. In Press.

O'Leary, P. and Harker, M. (2011). Polynomial approximation: An alternative to windowing in fourier analysis. *IEEE Proceedings of I2MTC 2011*.

Oppenheim, A. and Schafer, R. (1989). *Discrete-Time Signal Processing*. Prentice-Hall, Englewood Cliffs, NJ.

Press, W. H., Teukolsky, S. A., Vetterling, W. T., and Flannery, B. P. (2002). *Numerical Recipes in C++: The Art of Scientific Computing*. Cambridge University Press.

Zhang, L., Theurer, C. B., Gao, R. X., and Kazmer, D. O. (2005). Design of ultrasonic transmitters with defined frequency characteristics for wireless pressure sensing in injection molding. *IEEE Transactions on Ultrasonics Ferroelectrics and Frequency Control*, 52(8):1360–1371.